Viscous elongation of glass rods: Experiments, simulations, and analysis

T. Irisawa,[1,a)] G. S. Cargill III,[1,b)] K. J. Hwang,[2] and A. M. Maniatty[3]
[1]*Department of Materials Science and Engineering, International Materials Institute for New Functionality in Glass, Lehigh University, Bethlehem, Pennsylvania 18018, USA*
[2]*Department of Chemical Engineering, Materials Science, and Mining Engineering, Columbia University, New York, New York 10027, USA*
[3]*Department of Mechanical, Aerospace, and Nuclear Engineering, Rensselaer Polytechnic Institute, Troy, New York 12180, USA*

(Received 28 July 2010; accepted 2 September 2010; published online 7 December 2010)

Viscous elongation of glass rods has been investigated to improve procedures for producing parabolic capillaries from straight capillaries for use as intensity concentrating x-ray optical elements. Experiments and simulations have been carried out pulling Corning 7740 borosilicate glass rods in a cylindrical furnace. Simulations were based on one-dimensional and two-dimensional finite difference/element calculations, assuming that deformation occurred by linear viscous flow and that the temperatures in the glass remained in equilibrium with the temperatures measured along the axis of the furnace. Rates of elongation in experiments were smaller than those in simulations for later stages of the elongation process. Further experimental and analytical investigations ruled out explanations based on increased viscosities caused by structural relaxation or by partial crystallization and showed that the simulations gave incorrect results because they did not incorporate the dependence of local heat transfer processes on the glass rod radius. © *2010 American Institute of Physics*. [doi:10.1063/1.3512961]

I. INTRODUCTION

Shaped glass capillaries have been used to confine and focus x-rays emitted from conventional or synchrotron sources by total reflection of the x-rays from the inner walls of the capillaries.[1–7] For a parabolic capillary and incident x-rays parallel to the capillary axis, the emitted x-rays are expected to be concentrated and to form a focal spot.[7] Shaped capillaries for x-ray optical elements have been formed from straight capillaries by controlled viscous deformation using local heating and uniaxial tensile loading. Bilderback *et al.*[4] have used a fixed cylindrical furnace and computer controlled loading forces to control the shape of capillaries. Hwang *et al.*[8] have used computer controlled furnace translations with a fixed loading force, including a computer simulation program to predict capillary shapes for differently programmed furnace translations. This paper describes experiments and simulations for shaping glass rods or capillaries using local heating and uniaxial tensile loading.

II. DESCRIPTION OF MATERIALS AND EXPERIMENTS

In the present experiments, 3 mm diameter Corning 7740 borosilicate glass rods were used in place of 3 mm outer diameter, 25 or 100 μm inner diameter, capillaries, also made of Corning 7740 borosilicate glass that were to be formed as x-ray optical elements. Deformation behavior of the rods and capillaries have been found to be nearly identical,[8] and the rods cost much less than the capillaries.

The reported temperature-dependent shear viscosity $\eta(T)$ for Corning 7740 borosilicate glass is shown in Fig. 1 and can be well represented by[9]

$$\eta(T) = 8.15 \times 10^{-11} \exp\left(\frac{4.22 \times 10^4 \text{ K}}{T}\right) \text{Pa s}, \quad (1)$$

which is plotted in Fig. 1.

The equipment used for the elongation studies shown in Fig. 2 consists of a resistively heated cylindrical furnace, a K-type thermocouple attached to the inner wall of the furnace near its center, and an variable voltage ac power supply. Overall dimensions of the cylindrical furnace were 65 mm outer diameter, 13 mm inner diameter, and 140 mm length. The furnace was mounted on 300 mm vertical motorized, computer controlled translation stage. The translation stage was used to map out the temperature distribution along the axis of the furnace, as noted below. Computer-controlled translation of the furnace during capillary elongation has also been used to produce parabolic profiles for x-ray focusing optics.[8]

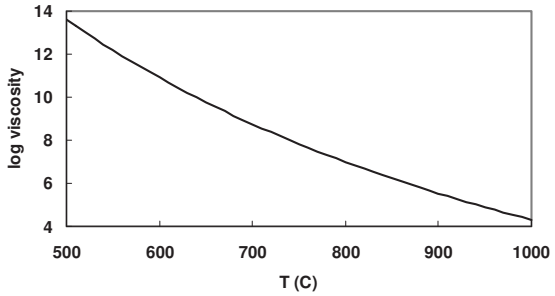

FIG. 1. Temperature-dependent viscosity for Corning 7740 borosilicate glass from Eq. (1).

[a)]Also at: Faculty of Science, Gakushuin University, Tokyo 171–8588, Japan.
[b)]Electronic mail: gsc3@lehigh.edu.

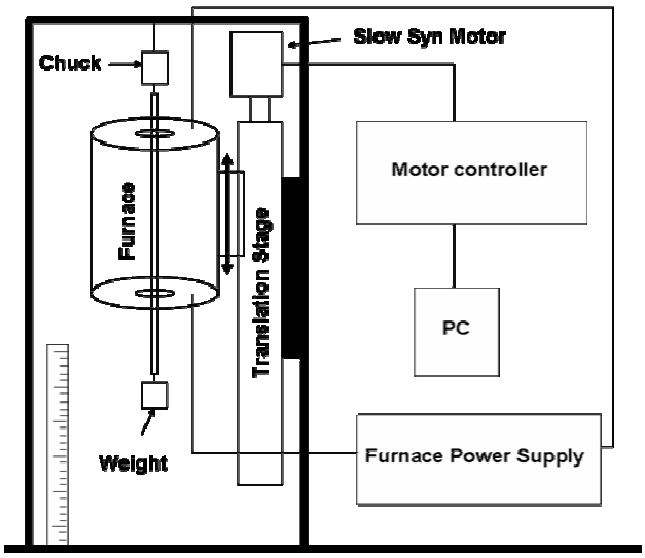

FIG. 2. Schematic description of equipment used in elongation studies.

The temperature along the axis of the furnace was measured using a K-type thermocouple in a 0.5 mm inner diameter, 2 mm outer diameter silica capillary that was translated along the axis of the furnace, while recording the thermocouple output and the position of the thermocouple junction within the furnace. Silica was used because it has much higher viscosity than borosilicate glass for the range of temperatures used in these experiments, so the silica capillary would not deform during the temperature measurements. The temperature measured by the thermocouple attached to the inner wall of the furnace near its center as a function of the supplied ac voltage is shown in Fig. 3. These temperatures are referred to as "set point temperatures" for each furnace voltage setting.

Distributions of temperature measured along the axis of the furnace are shown in Fig. 4 as a function of the distance from the top of the furnace. As expected, the temperature is highest near the middle of the furnace. The shape of the temperature distribution is very similar for different furnace voltages. Black and white dots were obtained at set point temperatures of 328 °C and 642 °C, respectively. The vertical axis on a left (right) side denotes the temperatures at the set-point temperature 328 °C (642 °C).

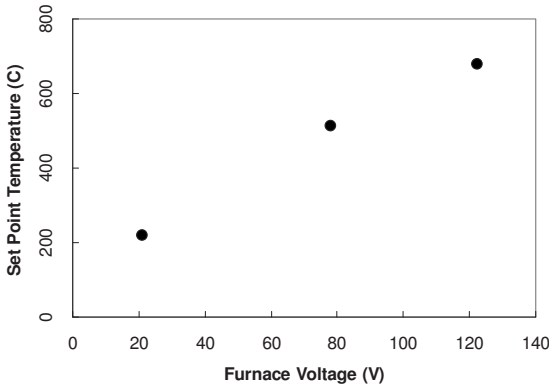

FIG. 3. Temperature measured at the inner wall near the center of the furnace as a function of the supplied ac voltage.

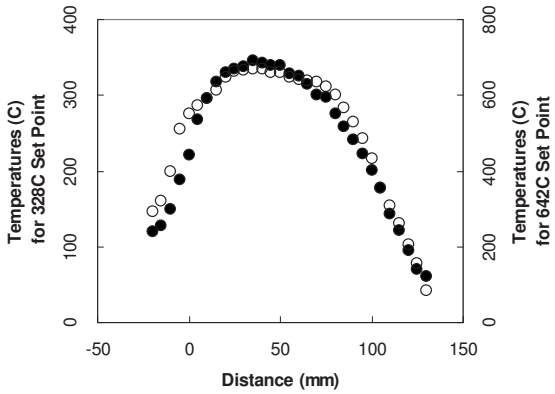

FIG. 4. Temperature distributions along the axis of the furnace obtained at set point temperatures of 328 °C (●) and 642 °C (○).

For the glass rod elongation experiments, a 40 cm long rod was inserted in the furnace, held at its top end by a cylindrical chuck. The furnace voltage was selected to obtain the desired set point temperature. After sufficient time for the glass rod and furnace to reach steady state temperatures, a cylindrical chuck was attached to the bottom end of the rod, with a chosen, additional weight suspended from the chuck. The total weight applied to the glass rod was given by the sum of the weight of the chuck plus that of the additional weight. The rod length was then monitored as a function of time. After the elongation reached a chosen value, the weighted chuck was removed from the rod, and the rod was removed from the furnace. The rod diameter was then measured as a function of distance along the length of the rod.

III. RESULTS FROM ELONGATION EXPERIMENTS

Experiments were carried out for three different set point temperatures, 712, 731, and 760 °C, using the same 46.8 g applied weight. The measured elongation lengths as a function of time are shown in Fig. 5. For all of the measurements elongation begins at time=0 s. As expected, the elongation rate is higher for the higher temperatures. These data show nearly linear initial increases in elongation lengths with time, followed by decreasing elongation rates.

Elongation lengths were also measured as a function of time for the same set point temperature, 760 °C, and for three different applied weights, 46.8, 71.8, and 96.8 g. Nor-

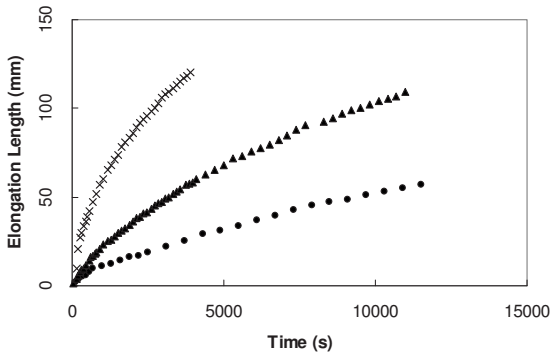

FIG. 5. The elongation length as a function of time for different set point temperatures, 712 °C (●), 731 °C (▲), and 760 °C (×) but with the same 46.8 g applied weight.

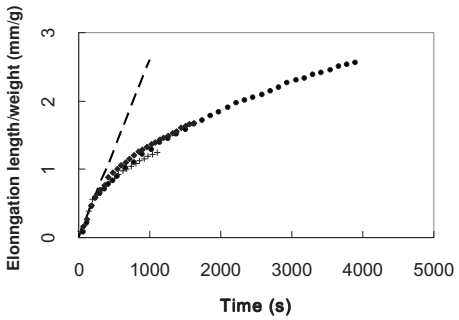

FIG. 6. Elongation lengths normalized by weights as a function of time for various applied weights, 46.8 g (●), 71.8 g (♦), and 96.8 g (+), for set point temperature of 760 °C. The dashed line indicates the initial elongation rate normalized by the applied weight 2.6×10^{-4} cm/s g.

malizing the elongation lengths by dividing the lengths by the applied weight for each of the three data sets gives the plots of normalized elongation length versus time in Fig. 6. These data demonstrate the elongation rate is proportional to the applied weight, and that the initial elongation rate normalized by the applied weight is 2.6×10^{-4} cm/s g for the set point temperature of 760 °C.

The measured outer diameter profiles of tapered glass rods as a function of distance along the rod length for a weight of 46.8 g and set point temperatures of 712, 731, and 760 °C are shown in Fig. 7. The measured outer diameter profiles of tapered glass rods as a function of the distance with weights 46.8, 71.8, and 96.8 g for a set point temperature of 760 °C are shown in Fig. 8. These data show that the diameter profiles were nearly independent of set point temperatures and weights. The profiles depended mainly on the total elongation length, rather than on the elongation rates.

IV. DESCRIPTION OF SIMULATIONS

A. Initial uniaxial elongation rate

The initial elongation rate, when the rod has not started to deform significantly, can be determined analytically with respect to the initial geometry assuming a uniaxial tensile stress along the rod. The uniaxial tensile stress σ_{zz} and tensile strain ε_{zz} are related to the viscosity η,[10,11]

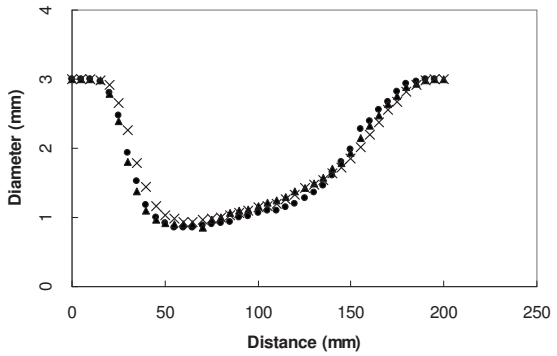

FIG. 7. Diameter profiles of tapered glass rods as a function of a distance with a weight of 46.8 g and for set point temperatures 712 °C (●), 731 °C (▲), and 760 °C (×).

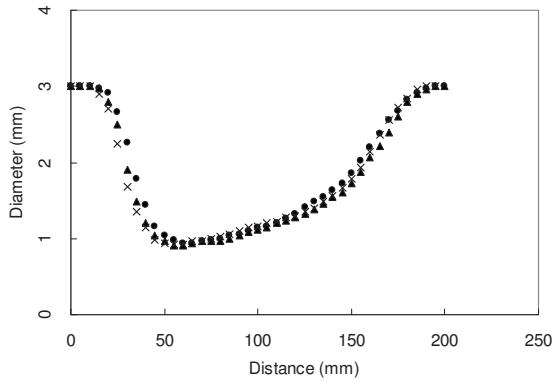

FIG. 8. Diameter profiles of tapered glass rods as function of the distance for a set point temperature of 760 °C and for applied weights 46.8 g (●), 71.8 g (▲), and 96.8 g (×).

$$\frac{d\varepsilon_{zz}(z)}{dt} = \frac{1}{3\eta(z)}\sigma_{zz}(z), \tag{2}$$

for a linear, incompressible, viscoelastic fluid, where z is the axis along the rod/capillary. To model deformation of glass rods and capillaries, the length as a function of time L(t) for a given initial uniform cross-sectional area A_0 and applied tensile force F was calculated as a function of time t during viscous flow. Since the temperature and viscosity depend on position along the axis of the furnace, elongation and shaping of glass rods and capillaries occur by nonuniform deformation. However, the initial rate of elongation can be calculated easily from the temperature distribution along the furnace axis T(z), the temperature-dependent viscosity η(T), the applied weight or mass m, resulting in force F=mg, where g=9.81 m/s^2, the rod's initial length L_0 and cross-sectional area A_0 or diameter d_0, and the density of the glass ρ.

For L_0=40 cm, d_0=3 mm, ρ=2.23 g/cm^3, and m =71.8 g, the initial, uniaxial stress distribution in the rod is

$$\sigma_{zz}(z) = \frac{F(z)}{A_0} = \frac{mg + (L_0 - z)A_0\rho g}{A_0} = \frac{mg}{A_0} + (L_0 - z)\rho g, \tag{3a}$$

$$\sigma_{zz}(z) = 99\ 646\ \text{Pa} + (40\ \text{cm} - z)(218.76\ \text{Pa/cm}), \tag{3b}$$

where z is measured from the top of the rod, is taken to be positive in the downward direction, and is in cm. In Eqs. (3a) and (3b), the weight of the rod itself is also included in the force F, which contributes less than 10% to the value of $\sigma_{zz}(z)$. The viscosity depends on z through position dependence of the temperature T(z). A polynomial fit T(z) was made to the measured temperature distribution corresponding to set point temperature of 760 °C, as shown in Fig. 9,

$$T(z) = 777.79 + 78.057z - 4.221z^2 - 0.19z^3\ \text{K} \quad \text{for}\ 0\ \text{cm} \le z \le 15.3\ \text{cm},$$

$$T(z) = 300\ \text{K} \quad \text{for}\ 15.3\ \text{cm} \le z \le 40\ \text{cm}. \tag{4}$$

The temperature-dependent glass viscosity was represented by Eq. (1). The resulting z-dependent strain rate $(d\varepsilon_{zz}(z)/dt)$ may then be determined by substituting Eqs. (1), (3b), (4),

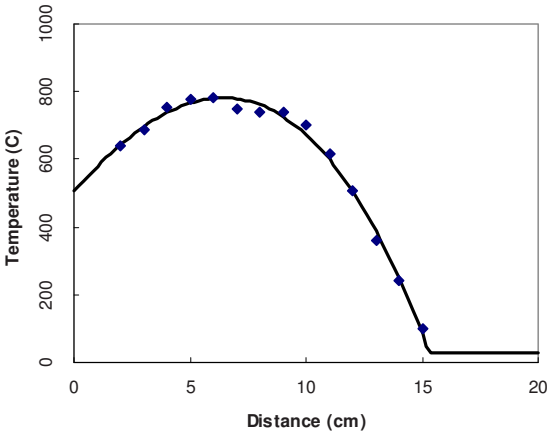

FIG. 9. (Color online) Comparison of experimentally measured temperature profile (♦) and the best-fit polynomial representation Eq. (4) (line) for a set point temperature of 760 °C.

and (5) into (2) and is show in Fig. 10. The initial rate of elongation is given by

$$\frac{dl}{dt} = \int_0^t \frac{d\varepsilon_{zz}(z)}{dt} dz = 5.85 \times 10^{-3} \text{ cm/s}, \quad (5)$$

or $(dl/dt\ m) = 0.81 \times 10^{-4}$ cm/s g, which is about three times smaller than the observed elongation rates shown in Fig. 6, $(dl/dt\ m) = 2.6 \times 10^{-4}$ cm/s g.

Because of the very strong dependence of the viscosity on temperature, only a few percent difference in the maximum absolute temperature causes large changes in the calculated elongation rate, as shown in Fig. 11. An increase in about 3%, or 32 °C, in the maximum temperature gives agreement between the calculated and measured initial elongation rates.

B. Longer time uniaxial elongation

For simulation of longer time uniaxial elongation, it is necessary to consider the change in cross-sectional area and position of material elements along the z axis as the capillary deforms. If the stress is assumed to be primarily uniaxial and not varying in the radial direction, a one-dimensional finite difference simulation, updating and tracking the position and cross-section of each material element along the z axis is

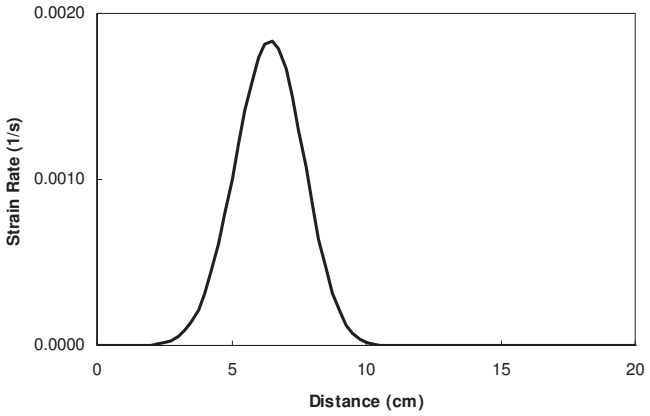

FIG. 10. Initial strain rate profile for 71.8 g weight and 760 °C set point temperature.

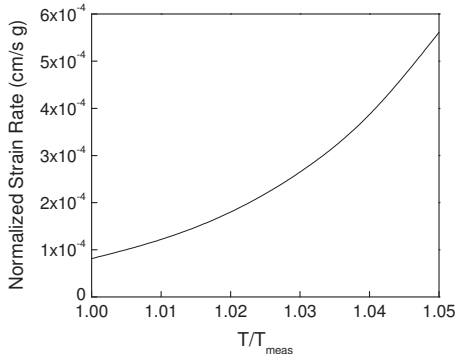

FIG. 11. Effect on the calculated initial elongation rate dl/dtm of increasing temperatures in Fig. 9 by a small multiplicative factor, corresponding to 0% to 5% temperature increases, for 760 °C set point temperature.

sufficient.[8] Inputs to the simulation are the temperature as a function of position z along the axis of the furnace T(z), the glass viscosity as a function of temperature $\eta(T)$, the applied tensile force F, the initial cross-sectional area A_0, the element length ΔL, the time step Δt, and the final length L_{max}. For the calculation, the section of the glass capillary or rod within the furnace length $L_F = 14$ cm is divided into a grid of $n = (L_F/\Delta L) = 60$ elements, each with the same length ΔL and initial cross-sectional area A_0 but with different temperatures and viscosities. Each element is deformed based on Eq. (2) for time steps $\Delta t = 1$ s. Smaller time intervals are used in latter stages of the elongation.

After each deformation step, all elements have different lengths and cross-sectional areas but all maintain the same volume $\Delta L A_0$. The deformed structure is then regrided to be described by new elements with the initial lengths ΔL and recalculated areas, and radii, that reflect the local deformation that has taken place. New elements are defined for segments of the rod that have left the furnace. Further deformation steps with new elements and regriding are performed until the simulated glass has deformed to the specified final length. The outputs of the simulation are the total glass length as a function of time and the final glass profile, or radius, as a function of position z.

To verify that the uniaxial simulation was adequate, two-dimensional (2D) axisymmetric finite element simulations were also performed, and the radial, circumferential, and shear stresses were computed throughout the rod.[12] The rod was modeled using 1000 eight-noded quadrilateral finite elements, 500 along the length and two in the radial direction. The velocities were computed at the nodes and the nodal positions were updated using a central difference scheme. A time step of 2.5 s was found to give converged results. Mesh convergence was also verified. Results for elongation versus time are shown in Fig. 12, which agree with the simple, short time simulation initially, and also agree with the long time uniaxial simulation.

The long time one-dimensional, uniaxial simulation, and 2D axisymmetric finite element method (FEM) simulation give nearly identical results because the σ_{zz} stress component is much larger than all the other stress components, so the stress state is nearly uniaxial, even with significant necking. Stress components along the axis of the rod are shown in

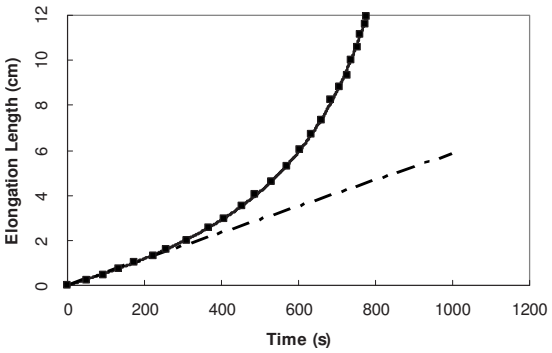

FIG. 12. Elongation vs time from one-dimensional (uniaxial) calculation (solid line) and from 2D FEM calculation (■), and initial elongation vs time from Eq. (5), for m=71.8 g and 760 °C temperature set point.

Fig. 13 at an elongation of 9 cm. A large increase in the axial stress develops at the neck due to the reduced cross-section area.

V. COMPARISONS OF RESULTS FROM SIMULATIONS AND EXPERIMENTS

Comparisons between one-dimensional (uniaxial stress) and 2D simulation results for elongation versus time are shown in Fig. 14, together with experimental results with the same elongation force F and temperature profile T(z) used in the simulations, with temperatures in simulations increased by ΔT=33 °C to give the observed initial elongation rate.

As shown in Fig. 14(a), elongation versus time results from simulations and experiments agree well for short times and small amounts of elongation but they diverge for longer times and longer elongations. These same data, plotted as elongation rate versus time in Fig. 14(b), show that the simulations predict that the elongation rate continues to increase, as the rod continues to elongate and to neck down but the experimental data show that the elongation rate actually decreases continuously.

The simulation results agreed reasonably well with observed radius profiles, as shown in Fig. 15, except that the profiles from simulations are somewhat deeper, with more necking, than in the experiments. However, there were very large, systematic differences between simulation and experimental results for elongation versus time, as seen in Fig. 14.

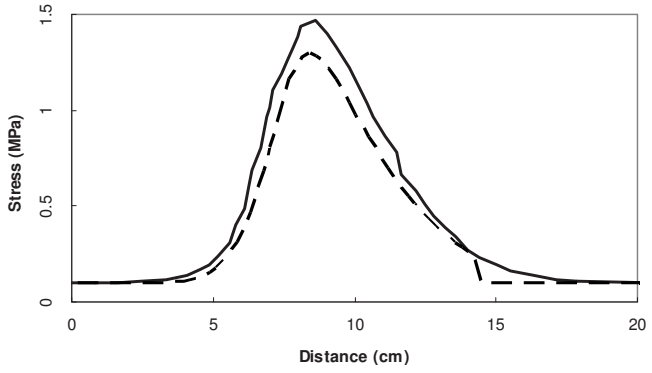

FIG. 13. Axial stress σ_{zz} from 2D FEM calculation (solid line) and from one-dimensional uniaxial simulation (dashed line), for m=71.8 g and 760 °C temperature set point. Other stress components from FEM calculation are smaller than 0.01 MPa and could not be seen in this plot.

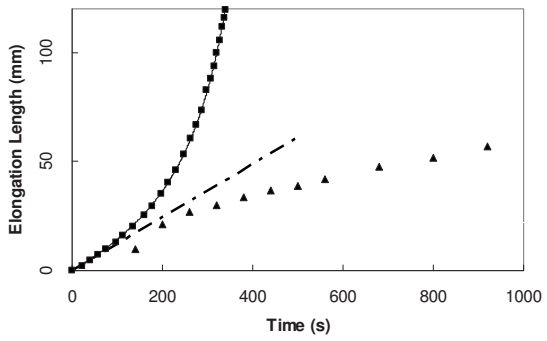

(a)

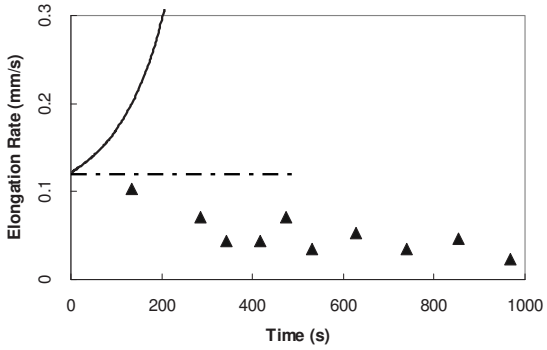

(b)

FIG. 14. (a) Comparison of one-dimensional (uniaxial) simulation (solid line) and 2D FEM (■) results and experimental results for glass rod elongation vs time with m=46.8 g and 760 °C set point temperature. The temperatures for the simulations were increased from those shown in Fig. 9 by ΔT=33 °C so that the simulations give the same initial elongation rate, 2.6×10^{-4} cm/s g (dashed-dotted-dashed line), as shown by the experimental data in Fig. 6 for 760 °C set point temperature. (b) Comparisons for elongation rates from simulations (solid line), from experimental results (▲), and from initial elongation rate calculation (dashed-dotted-dashed line).

Note that the simulations predict elongation rates strongly increasing with time but experiments show elongation rates weakly decreasing with time and then becoming nearly constant.

VI. INVESTIGATION OF POSSIBLE REASONS FOR DISAGREEMENTS BETWEEN SIMULATION AND EXPERIMENTAL ELONGATION RATES

Three different possibilities were investigated as causes for the large differences between simulation and experimen-

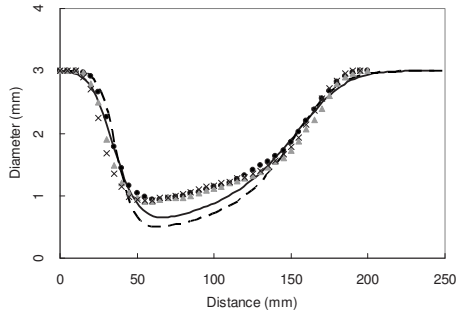

FIG. 15. Experimental diameter vs distance profiles from Fig. 8 for set point temperature of 760 °C for applied weights 46.8 g (●), 71.8 g (▲), and 96.8 g (×), and one-dimensional uniaxial simulation result for m=71.8 g and 760 °C set point temperature (solid line) and with ΔT=33 °C (dashed line) as in Fig. 14.

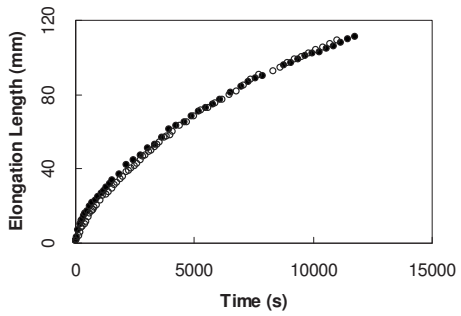

FIG. 16. The elongation length as a function of the time measured with a weight of 46.8 g and a maximum furnace temperature of 731 °C. The symbols ● and ○ correspond to the annealed glass rod (731 °C, 4 h) and unannealed glass rod, respectively.

tal results for elongation versus time: (1) failure properly to include triaxial stress effects in simulations, (2) changes in glass viscosity versus temperature behavior caused by glass relaxation or by partial crystallization during the elongation process, and (3) inaccuracy or inapplicability of temperature versus position measurements made along the axis of the cylindrical furnace. Results of these investigations are described in this section. The close agreement between the one-dimensional uniaxial simulation results and the 2D FEM results, which include full triaxial stress effects, indicate that the latter are not responsible for the failure of simulations to predict the observed long-time elongation rates. Results concerning the other two possibilities are described below.

A. Changes in glass viscosity

There are several reports that the viscosity of glass can be increased by annealing, and structural relaxation, at higher temperatures.[13–15] Also, annealing might lead to partial crystallization and increased effective viscosity. In order to determine whether either of these phenomena might be responsible for the difference between simulation results and experimental results in Fig. 14, the effects of annealing on viscosity were investigated for the glass rods used in the elongation experiments. Glass rods were annealed, and then the rates of viscous elongation were measured.

The elongation rate of an unannealed glass rod was compared with that for a rod that had been annealed for 4 h at 731 °C. The measurements were made for a weight of 46.8 g and a maximum furnace temperature of 731 °C. Figure 16 shows that the elongation lengths as a function of the time for the annealed glass rod and for the unannealed glass rod were identical. Any changes in the viscosity caused by annealing were too small to affect the viscous elongation rate under these experimental conditions. These results demonstrate that annealing-induced viscosity changes, due to structural relaxation or to partial crystallization, could not be responsible for the difference between experimental and simulation results like those shown in Fig. 14.

B. Temperature changes during elongation

An important input to the simulations is the temperature distribution T(z) along the axis of the cylindrical furnace, which was assumed to correspond to the temperature distribution of the glass rods within the furnace. Experiments were carried out to determine whether shape and dimensional changes in the glass during viscous elongation may be affecting heat transfer between the glass in the furnace, the furnace itself, and the parts of the glass that extend outside of the furnace. Such changes in heat transfer might cause the temperature distribution in the elongating rod to differ from that determined using a straight, nondeforming capillary. Because glass viscosity is highly temperature dependent, changes in the temperature of the glass during elongation could strongly affect elongation rates.

To determine the behavior of the temperature of the glass during elongation, Corning 7740 borosilicate glass capillary tubing with 6.5 mm outside diameter and 1 mm inside diameter, was used in place of the 3 mm diameter glass rods to permit a type K thermocouple to be contained within the larger diameter capillary tubing, with the thermocouple junction located at the center of the cylindrical furnace. Elongation rates and temperatures were monitored with no weight attached to the bottom end of the glass rod, or with weights of 169 and 216 g. Initial capillary lengths were 300 or 1000 mm.

In these experiments, the glass capillaries were hung in the cylindrical furnace and weights were attached when the furnace was at room temperature, before applying voltage to the furnace. Voltage was then applied and increased, to bring the nominal maximum furnace temperature to about 688 °C. The nominal maximum furnace temperature T_{center} was read from a type K thermocouple in contact with the outer wall of the 13 mm inner diameter ceramic tube surrounded by a nichrome resistance heater, glass wool insulation, and a 65 mm diameter metal tube enclosure. The thermocouple within the bore of the capillary tube, with its junction at the center of the furnace, was used to obtain the maximum capillary temperature $T_{capillary}$, as the capillary elongated, similar to the elongation and tapering of the 3 mm diameter rods used in the earlier experiments.

The most rapid elongation occurred at the furnace center, where the temperature was highest and where the thermocouple junction was located. As shown in Figs. 17(a)–17(c), the temperature $T_{capillary}$ initially increased faster than the temperature T_{center}, to a maximum value of about 745 °C, nearly 60 °C higher than T_{center}.

For case (e), with no weight attached, only 4 mm elongation occurred, and after an initial 10 °C drop in $T_{capillary}$, from 758 °C at t=1980 s to 748 °C at t=2700 s, the maximum capillary temperature decreased by only 7 to 741 °C, at t=9240 s. During this time, T_{center} remained nearly constant at 690 °C.

Very different behaviors were observed for cases (a) and (b), where attached weights caused large elongations ΔL of 64 mm and 119 mm, respectively, which were accompanied by drops in $T_{capillary}$ from 745 °C to 694 °C and 680 °C, respectively. As seen in Figs. 17(c) and 17(d), the dependence of $\Delta T_{capillary}$ on elongation ΔL is nearly linear, with the rate of decrease being somewhat greater for case (b) with the 1000 mm initial length than for case (a) with the 300 mm initial length.

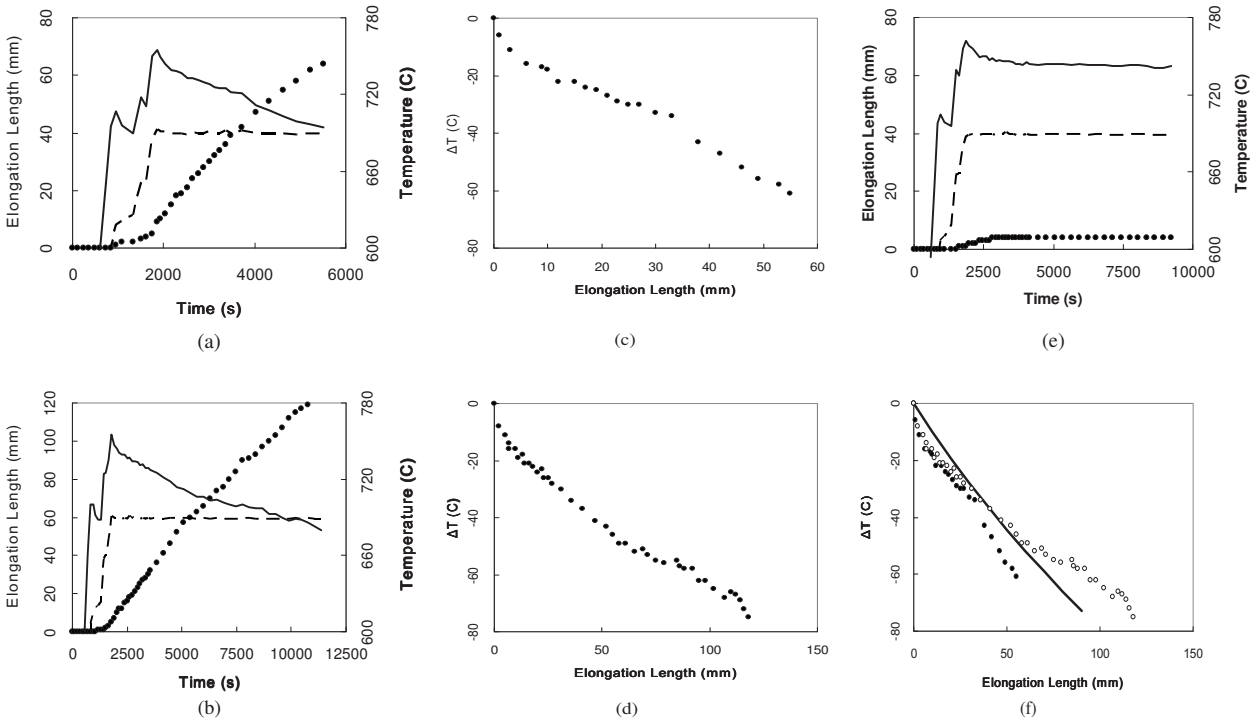

FIG. 17. Results of capillary elongation experiments. (a) and (b) show elongation length (●), nominal furnace temperature maximum T_{center} (dashed line) and maximum capillary temperature $T_{capillary}$ (solid line) as functions of time t, for (a) 300 mm initial length and 216 g weight and (b) 1000 mm initial length and 169 g weight. (c) and (d) are plots of the changes in maximum capillary temperature vs elongation length from the time of maximum $T_{capillary}$ for the cases shown in (a) and (b), respectively. (e) shows the same measurements as (a) and (b) but for 300 mm initial length and no attached weight. (f) compares of rates of temperature decrease for cases (a) and (b) (data points) with results of a simple heat transfer calculation (solid line) described in Sec. VII.

The elongation versus time behaviors in Figs. 17(a) and 17(b) are similar to those shown in Figs. 5, 6, 14, and 16, with the elongation rates decreasing with time, rather than increasing with time as expected from simulations. The decrease in $T_{capillary}$ with time, and with elongation, shown in Figs. 17(c) and 17(d), provides an explanation of this difference, since in the simulations the capillary temperature is assumed to depend only on the position along the furnace length and not to change with time, as indicated by the experimental results shown in Fig. 17.

VII. ANALYSIS OF HEAT TRANSFER EFFECTS IN GLASS ROD ELONGATION

In order to understand the cause for the observed decrease in $T_{capillary}$ with time, and with elongation, we have carried out a simplified analysis of the factors that determine $T_{capillary}$ and its dependence on capillary diameter, length, and elongation. Our treatment is similar to approach described by Paek and Runk.[16]

For simplicity, and as shown in Fig. 18(d), the temperature of the inner furnace wall is assumed to be constant T_F over the full length of the furnace L_0. T_0 is the temperature outside of the furnace. T_G is the temperature of the glass in the necked down region with radius R, which extends through the full length of the furnace. The circumference of the rod in the necked down region is $2\pi R$. The original rod radius is R_0, so the original cross section area is $A_0 = \pi R_0^2$.

The equation relating the temperature in the glass $T_G(z)$ to the furnace wall temperature T_F and the radius of the glass in the neck down region R is

$$K_{eff}\left|\frac{dT_G(z)}{dz}\right| 2A_0 = (2\pi R)\varepsilon\sigma(T_F^4 - T_G^4)L_0, \quad (6)$$

where K_{eff} is the thermal conductivity of the glass, ε is the emissivity, and σ is the Stefan–Boltzmann constant. The term on the left hand side of Eq. (6) represents heat flow from the neck down region to the glass outside of the top and bottom ends of the furnace. In Eq. (6) the same cross section

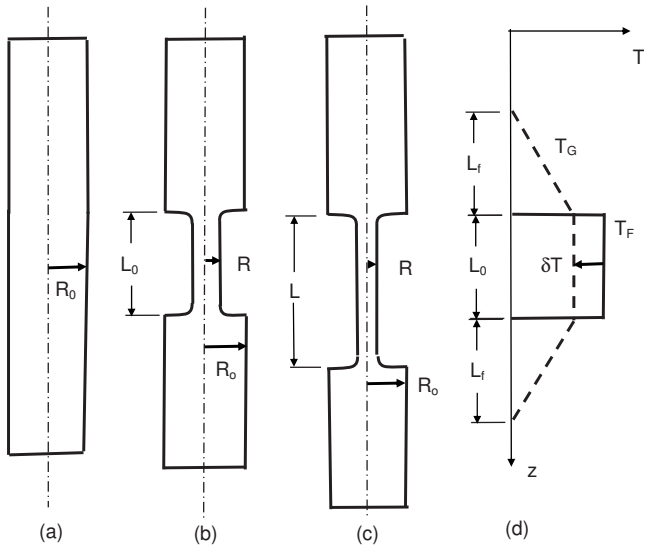

FIG. 18. Cross-sections of glass rod before elongation (a) and during elongation (b) and (c), and temperature distribution of the furnace wall T_F and of the glass rod T_G (d). Note the necked down region of reduced radius R in (b) and (c).

area A_0 is used for the top and bottom ends, although as shown in Fig. 18(c), in the later stages of elongation the cross section area will be smaller than A_0 for the bottom end. This simplification will affect the quantitative results but should not change the qualitative dependence of T_G on R. The term on the right hand side of Eq. (6) represents heat flow from the inner furnace wall at temperature T_F to the glass rod at temperature T_G. The dependence of T_G on R comes mainly from this term because of the decrease in the circumference of the glass rod as elongation decreases its radius, which reduces heat flow from the furnace walls to the glass.

The derivative $|(dT_G(z)/dz)|$ is approximated as $T_G - T_0/L_f$, where L_f is the distance over which the temperature of the glass drops from T_G inside of the furnace to T_0 outside of the furnace. To simplify numerical evaluations, L_f is taken to be the same as L_0, as shown in Fig. 18(d),. The temperature of the glass inside of the furnace T_G is assumed to be uniform along the length L_0 of the glass rod contained within the furnace. Introducing δT as the difference in temperature between the glass in the furnace and the inner wall of the furnace, $T_F = T_G - \delta T$, Eq. (6) can be simplified for $|\delta T| \ll T_F$ and $|\delta T| \ll T_G$, to yield

$$\delta T(R) = \frac{-\frac{A_0 2K_{eff}}{L_F}(T_F - T_0)}{\frac{A_0 2K_{eff}}{L_F} + (8\pi L_0 \varepsilon \sigma T_F^3)R}, \tag{7}$$

or

$$\delta T(R) = \frac{T_0 - T_F}{1 + \left(\frac{4\pi L_0 L_F \varepsilon \sigma T_F^3}{A_0 K_{eff}}\right)R}. \tag{8}$$

Equation (8) can be further simplified if $(4\pi L_0 L_F \varepsilon \sigma T_F^3 / A_0 K_{eff})R \gg 1$, yielding

$$\delta T(R) = \frac{A_0 K_{eff}}{4\pi L_0 L_F \varepsilon \sigma T_F^3}\frac{(T_0 - T_F)}{R}. \tag{9}$$

With approximate numerical values, $R_0 = 0.3$ cm, $A_0 = 0.3$ cm^2, $L_0 = 6$ cm, $L_F = 6$ cm, $\sigma = 6 \times 10^{-12}$ (W/cm^2 K^4), $\varepsilon = 0.5$, $K_{eff} = 0.3$ W/cm K, $T_F = 1100$ °C,

$$\frac{A_0 K_{eff}}{4\pi L_0 L_F \varepsilon \sigma T_F^3}\frac{1}{R_0} = 0.16, \tag{10}$$

and

$$\delta T(R) = 0.16\frac{R_0}{R}(T_0 - T_F). \tag{11}$$

From Eq. (11), $\delta T = (T_G - T_F) < 0$, the difference between the glass temperature and the furnace wall temperature, is expected to become more negative, the temperature of the glass dropping, as the glass radius decreases.

To compare with the experimental results in Figs. 17(a)–17(d), a relation is needed between the glass radius R and the elongation ΔL, which obtained assuming conservation of volume, with the elongation corresponding to the length of the necked down region,

$$R(\Delta L) = \frac{R_0}{\sqrt{1 + \frac{\Delta L}{L_0}}}. \tag{12}$$

With this substitution, Eq. (11) becomes

$$\delta T(\Delta L) = -125\sqrt{1 + \frac{\Delta L}{L_0}}. \tag{13}$$

For $\Delta L = 0$, $\delta T = -80$ K. With increasing ΔL, δT becomes more negative. Defining the difference between the temperature of the glass for $\Delta L = 0$ and the temperature of the glass for $\Delta L > 0$,

$$\Delta T(\Delta L) = \delta T(\Delta L) - \delta T(\Delta L = 0), \tag{14}$$

gives

$$\Delta T(\Delta L) = -125\left(1 - \sqrt{1 + \frac{\Delta L}{L_0}}\right), \tag{15}$$

so for $\Delta L = 0$, $\Delta T = 0$, and ΔT becomes more negative as ΔL increases.

A closed form solution for the temperature distribution in a stepped cylinder in a uniform temperature furnace, the situation represented by Figs. 18(b) and 18(c), with the requirements of temperature and heat flow being continuous at the steps $z = \pm(L_0/2)$, can be obtained.[17] From that analysis, the deviation δT of the temperature of the glass from that of the furnace at $z = 0$ becomes smaller, the glass becoming hotter, approaching $\delta T = 0$ as the radius R of the stepped down region becomes smaller, in contrast with the result of Eq. (9) that the temperature difference $\delta T(R)$ increases, the glass becoming cooler, with decreasing R. The assumption used to obtain Eq. (9), that $|(dT_G(z)/dz)| = (T_G - T_0/L_F)$ with constant L_F, is not satisfied in the closed form analysis.

The temperature decrease observed experimentally during neck down, which is predicted by the approximate analysis leading to Eqs. (9) and (15) and which can explain the observed decreasing elongation rates, may involve the actual peaked shape of the temperature distribution in the furnace and the continuous neck down changes in the shape of the rod, neither of which are included in the stepped cylinder model and which would make more accurate analysis much more difficult.

$\Delta T(\Delta L)$ from Eq. (15), plotted in Fig. 17(f), demonstrates that this simple heat transfer calculation reproduces the observed dependence of glass temperature on elongation, for reasonable values of the dimensional and thermal parameters. A more thorough treatment would require numerical analysis like that described by Paek and Runk.[16]

The decrease in glass temperature with increasing elongation predicted by Eq. (15) and observed experimentally, as shown in Fig. 17(f), is the most likely explanation for differences between simulation predications and experimental observations of elongation rates shown in Fig. 14.

Incorporation of a more realistic treatment of the relationship between the temperature of the furnace and the temperature of the glass should greatly improve the value of the simulations in optimizing conditions for production of tapered capillaries with desired shapes.

VIII. DISCUSSION AND CONCLUSIONS

This study of viscous elongation of glass rods has revealed an unexpected dependence of the glass rod's temperature on local rod diameter, which results in continuously *decreasing* elongation rate with time. One-dimensional and 2D simulations assuming that the temperatures in the glass remain in equilibrium with the temperatures measured along the axis of the cylindrical furnace predict continuously *increasing* elongation rate with time, as the rod local diameter decreases in the highest temperature region of the furnace. Nevertheless, the simulations give predictions of glass rod diameter profiles for different total elongations similar to those obtained experimentally, although the simulations over estimate the degree necking, i.e., they predict somewhat smaller minimum rod diameters than those observed.

Agreement between predictions of one-dimensional and 2D simulations, and the very small values of non-axial stresses indicated in the latter, confirm that the viscous deformation under these conditions is determined essentially by the axial stress. Absence of significant effects of preannealing on elongation rates rules out explanations based on increased viscosity caused by structural relaxation or by partial crystallization. More realistic modeling of viscous elongation of glass rods requires incorporation of improved treatment of heat transfer processes between the furnace and glass rod.

ACKNOWLEDGMENTS

Parts of this work were supported by the International Materials Institute for New Functionality in Glass with NSF Grant Nos. DMR-0409588 and DMR-0844014 at Lehigh University, by NSF Grant Nos. DMR-9896002 and DMR-9796284 at Columbia and Lehigh Universities, and by NSF Grant No. DMR-0312189 at Lehigh University and Rensselaer Polytechnic Institute. We are grateful to Dr. A. Alben for providing the closed form solution for the temperature distribution in a stepped cylinder discussed in Sec. VII.

[1]D. H. Bilderback, D. J. Thiel, R. Pahl, and K. E. Brister, J. Synchrotron Radiat. **1**, 37 (1994).
[2]K. F. Voss, K. H. Kim, E. A. Stern, F. C. Brown, and S. M. Heald, Nucl. Instrum. Methods Phys. Res. A **347**, 390 (1994).
[3]D. X. Balaic, K. A. Nugent, Z. Barnes, R. Garrett, and S. W. Wilkins, J. Synchrotron Radiat. **2**, 296 (1995).
[4]D. Bilderback, R. Pahl, and R. Freeland, CHESS Newsletter, p. 41 (1995).
[5]D. H. Bilderback, X-Ray Spectrom. **32**, 195 (2003).
[6]R. Huang and D. Bilderback, J. Synchrotron Radiat. **13**, 74 (2006).
[7]N. Schell, F. Eichhorn, A. Bjeoumikhov, H. Prinz, and C. Ollinger, *Ninth International Conference on Synchrotron Radiation Instrumentation*, edited by J.-Y. Choi and S. Rah (American Institute of Physics, Melville, NY, 2007), p. 975.
[8]K. J. Hwang, "Optimization of glass capillary production for x-ray microdiffraction," MS thesis, School of Engineering and Applied Science, Columbia University, 1997.
[9]*Handbook of Glass Manufacture*, edited by F. V. Tooley (Ashlee, New York, 1984), Vol. 2.
[10]O. V. Mazurin, J. Non-Cryst. Solids **87**, 392 (1986).
[11]D. B. Dingwell, *Mineral Physics and Crystallography: A Handbook of Physical Constants* (American Geophysical Union, Washington, 1995), p. 209.
[12]T. J. R. Hughes, *The Finite Element Method: Linear Static and Dynamic Finite Element Analysis* (Prentice-Hall, Englewood Cliffs, NJ, 1987).
[13]H. R. Lillie, J. Am. Ceram. Soc. **19**, 45 (1936).
[14]G. O. Jones, Rep. Prog. Phys. **12**, 133 (1949).
[15]G. W. Scherer, *Relaxation in Glasses and Composites* (Wiley, New York, 1986).
[16]U. C. Paek and R. B. Runk, J. Appl. Phys. **49**, 4417 (1978).
[17]R. Alben, private communication (9 September 2010).